Journal of Inflammation Research

Dovepress
Taylor & Francis Group

Open Access Full Text Article

ORIGINAL RESEARCH

Unveiling PANoptosis in Acute Kidney Injury: An Integrative Multi-Dimensional Approach to Identify Key Biomarkers

Ning Wang[1,*], Lina Zhang[1,2,*], Ziyu Xu[1,*], Qin Xu[1,2], Yanfang Lu[1,2], Peiyuan Niu[1,2], Lei Yan[1,2], Limeng Wang[1,2], Huixia Cao[1,2], Fengmin Shao[1,2]

[1]Department of Nephrology, Zhengzhou University People's Hospital, Henan Provincial People's Hospital, Zhengzhou, People's Republic of China; [2]Henan Provincial Key Laboratory of Kidney Disease and Immunology, Henan Provincial Clinical Research Center for Kidney Disease, Henan Provincial People's Hospital, Zhengzhou, People's Republic of China

*These authors contributed equally to this work

Correspondence: Limeng Wang; Fengmin Shao, Department of Nephrology, Zhengzhou University People's Hospital, Henan Provincial People's Hospital, Zhengzhou, People's Republic of China, Email wanglimeng668@126.com; fengminshao@126.com

Background: Programmed cell death and inflammatory responses are critical in the progression of acute kidney injury (AKI). PANoptosis, a highly regulated and complex form of programmed inflammatory cell death, integrates the molecular mechanisms of apoptosis, pyroptosis, and necroptosis. While this process has been implicated in various inflammatory conditions, its specific role in AKI remains unclear.

Methods: The role of PANoptosis in AKI was investigated using single-cell RNA sequencing (scRNA-seq) and bulk transcriptomic data. Initially, scRNA-seq was utilized to identify differentially expressed genes (DEGs) associated with apoptosis, pyroptosis, and necroptosis in individual AKI cells. Through integrating these DEGs, a candidate gene set associated with PANoptosis was established. Several machine learning algorithms were employed to determine the optimal feature genes. The diagnostic potential of these genes was examined through receiver operating characteristic curve analysis. Gene set enrichment analyses were performed to explore their relationship with PANoptosis. Further validation was carried out using AKI animal models.

Results: PANoptosis levels were significantly elevated in AKI. ScRNA-seq revealed heterogeneity in PANoptosis activity across cell types. Integration of transcriptomic data with machine learning algorithms led to the identification of five key upregulated genes: EGR1, CEBPD, HSPA1A, HSPA1B, and RHOB. The diagnostic potential of these genes was demonstrated with the area under curve values of 0.981 for EGR1, 0.920 for CEBPD, 0.968 for HSPA1A, 0.970 for HSPA1B, and 0.953 for RHOB. Functional enrichment analysis demonstrated a significant positive correlation between the expression of these biomarkers and PANoptosis activity. Validation through Western blot and immunohistochemistry further confirmed their roles in AKI pathogenesis.

Conclusion: By integrating scRNA-seq and transcriptomic data, along with the application of innovative methodologies, five key PANoptosis-related genes associated with AKI were identified. Our study offers new insights into the role of PANoptosis in AKI and highlights potential biomarkers for clinical evaluation and therapeutic targeting.

Keywords: acute kidney injury, PANoptosis, single-cell RNA sequencing, machine learning, biomarkers

Introduction

Acute kidney injury (AKI) is a multifactorial clinical condition marked by a swift increased in serum creatinine (SCr) levels and reduced in glomerular filtration rate.[1] This syndrome serves a crucial function in clinical settings, affecting approximately 20% of hospitalized patients, and is increasing annually.[2] Notably, in intensive care unit settings, the incidence of AKI has surpassed 50%.[3] It has a grim prognosis, elevating the likelihood of transitioning to chronic kidney disease, end-stage renal disease, cardiovascular complications, and mortality.[4,5] Despite extensive research, the exact

Received: 10 March 2025
Accepted: 27 June 2025
Published: 2 July 2025

etiological factors and pathogenic mechanisms of AKI remain unclear. As effective therapeutic strategies for AKI are currently lacking, identifying novel biomarkers and formulating tailored treatments for AKI are crucial.[6]

As the principal pathological feature of AKI is the death of proximal tubular (PT) cells, investigating it from the perspective of programmed cell death (PCD) represents a widely accepted research strategy.[7,8] Since the discovery of apoptosis as the first type of PCD, over ten other types have been identified, including pyroptosis and necroptosis.[9] Previous research suggested that different modes of cell death follow fixed, unique pathways and operate independently. However, subsequent studies have revealed extensive interactions between cell-death pathways. This understanding has given rise to the notion of PANoptosis, an inflammatory form of PCD governed by the PANoptosome, which necessitates the concurrent activation of apoptosis, pyroptosis, and necroptosis.[10–12] The PANoptosis concept highlights that targeting a single cell-death pathway is unlikely to yield desired therapeutic outcomes.[13,14] PANoptosis plays a pivotal role in the pathogenesis of AKI. In sepsis-induced AKI, the upregulation of EIF2AK2 enhances the expression of AIM2, thereby promoting PANoptosis in PT cells and exacerbating the progression of AKI.[15] Additionally, studies suggest that PSTPIP2 mitigates AKI by inhibiting PANoptosis in mouse renal tubular epithelial cells.[16] These findings suggest that therapeutic strategies targeting PANoptosis could partially alleviate kidney injury, underscoring its potential as a treatment target. Nevertheless, the current understanding of the regulatory processes and molecular mechanisms underlying PANoptosis in AKI remains limited.

While current research underscores the crucial role of PANoptosis in the pathogenesis and treatment of AKI, the identification and validation of key regulatory genes remain challenging. Traditional RNA sequencing (RNA-seq) methods often fail to capture cell-specific gene expression and activity changes, which are essential for understanding the heterogeneous regulation of PANoptosis in AKI. Recent advancements in single-cell RNA sequencing (scRNA-seq) have addressed this limitation, enabling both quantitative and qualitative analyses of cellular composition in complex tissues.[17] These advancements provide critical insights into cellular heterogeneity in AKI, facilitating a more precise characterization of disease features.[18] Furthermore, machine learning, a subset of artificial intelligence, can process large datasets and support tasks such as disease diagnosis and healthcare management.[19] By integrating machine learning with bioinformatics, the capabilities of scRNA-seq can be significantly enhanced, improving data analysis accuracy and further aiding the identification and investigation of potential diagnostic biomarkers.

In this study, scRNA-seq was employed to find differentially expressed genes (DEGs) associated with apoptosis, pyroptosis, and necroptosis in individual AKI cells. By analyzing these DEGs, we established a candidate gene set associated with PANoptosis. Multiple machine-learning algorithms were then applied to the bulk RNA-seq datasets, leading to the identification of optimal feature genes. These findings were additionally corroborated using animal experiments. The integration of scRNA-seq and bulk RNA-seq data, combined with machine learning, offers an innovative approach that enhances our understanding of PANoptosis in AKI and reveals potential new therapeutic targets.

Materials and Method

Data Source

The scRNA-seq data of 32 specimens including normal (n = 20) and AKI (n = 12) kidney tissue were procured from the Gene Expression Omnibus (GEO) database (https://www.ncbi.nlm.nih.gov/geo) with accession ID GSE183276.[20] We downloaded the bulk RNA-seq dataset GSE43974 from the GEO, which comprised 188 normal and 203 AKI samples.[21] All datasets used in this study were provided in Supplementary Table 1.

Lists of essential regulatory genes linked to apoptosis, pyroptosis, and necroptosis were included as PANoptosis-related genes, and gene lists were obtained from the GSEA gene set, KEGG, REACTOME, Hallmark, and previous study.[22] Ultimately, 577 apoptosis-, 49 pyroptosis-, and 100 necroptosis-related genes were analyzed (Supplementary Table S2). Gene set variation analysis (GSVA) was executed utilizing the ssGSEA R package to gauge the impact of PANoptosis on AKI and normal tissues on the GSE43974 dataset.[23]

Data Integration and Processing

The scRNA-seq data underwent processing via the Seurat R software.[24] Quality control criteria encompassed filtering cells with minimum expression in three cells, maintaining RNA features within the range of 200–7000 per cell, and ensuring that mitochondrial RNA content was less than 20% (Figure S1). In total, 25,684 eligible cells were retained for further analysis. Remaining cells underwent scaling and normalization using a linear regression model employing the "Log Normalization" technique. The top 3000 highly variable genes were identified using the "FindVariable-Features" function. Data were then downscaled using principal component analysis. The "Harmony" package was employed to eliminate batch effects between samples and prevent interference with downstream analyses. Cell types were annotated and then hand checked based on previous studies. Differential expression analysis of bulk RNA-seq data was executed utilizing the R package "limma".[25]

PANoptosis Activity

The scRNA-seq data was utilized to determine the gene sets associated with PANoptosis activity. The AUCell, UCell, singscore, ssgsea, and AddModuleScore algorithms were employed to assess the activities of apoptosis, pyroptosis, and necroptosis at the single-cell level, with overall activities computed through scoring.[26,27] Cells were categorized into elevated and reduced activity clusters according to the median score. DEGs between high- and low-activity cells were identified using the "FindMarkers" function. A list of candidate genes related to PANoptosis was generated by intersecting the DEGs from the three cell death pathways.

Functional Enrichment

To investigate the functions and mechanisms of potential PANoptosis-related genes, gene ontology (GO) and disease ontology (DO) enrichment analyses were conducted utilizing the "clusterProfiler" R package.[28]

Optimal Feature Genes

Seven machine-learning algorithms including eXtreme Gradient Boosting (XGBoost), Boruta, Random Forest (RF), Least Absolute Shrinkage and Selection Operator (LASSO), Support Vector Machine Recursive Feature Elimination (SVM-RFE), Decision Tree (DT), and Gradient Boosting Machine (GBM) were applied to identify core genes. Feature selection strategies were utilized to reduce the number of core genes, thereby identifying the optimal feature genes associated with PANoptosis in AKI.

LASSO introduces regularization into the loss function, improving both prediction accuracy and model transparency. To enhance robustness and avoid overfitting, we applied LASSO regression with 5-fold cross-validation. The RF method generates multiple decision trees through random sampling and feature selection, with final predictions based on either voting or averaging. For our random forest model, we used 500 trees and 10-fold cross-validation, which highlighted important feature interactions and correlations. The Boruta algorithm assesses feature importance by comparing original features with randomly shuffled versions, efficiently handling high-dimensional data without preprocessing or interference from feature correlations. XGBoost improves accuracy by iteratively training decision trees, with error corrections made in each iteration, while an early stopping strategy helps prevent overfitting. SVM-RFE identifies the most relevant features, discarding irrelevant ones to enhance both interpretability and robustness. GBM combines several weak learners into a robust predictive model, while DT splits data to maximize homogeneity within subsets. Optimal feature genes were identified by intersecting those identified by all seven algorithms.

Expression and Diagnostic Value of the Optimal Feature Genes

The manifestation of the most significant feature genes in the AKI specimens was validated utilizing the Wilcoxon rank-sum test. The diagnostic performance of these genes was evaluated by computing the area under the receiver operating characteristic (ROC) curve. Correlation analysis identified relationships between core genes and apoptosis, pyroptosis, and necroptosis. Furthermore, the manifestation of core apoptosis, pyroptosis, and necroptosis genes in the high- and

low-activity cohorts was examined and visualized using ggplots. The abundance levels of the optimal feature genes at the single-cell level were illustrated using UMAP plots.

Gene Set Enrichment and Correlation Analyses

Gene Set Enrichment Analysis (GSEA) was executed on feature genes to evaluate their association with apoptosis, pyroptosis, and necroptosis, as well as potential regulatory mechanisms. Pearson correlation analysis was employed to measure the relationships between gene expression levels and PANoptosis.

AKI Mouse Model

Male C57BL/6J mice (specific pathogen-free, 6–8 weeks old, weighing 20–25 g) were procured from Jiangsu Jicuiyaokang Biotech Co. (Jiangsu, China). The modeling methods and evaluation criteria were derived from the framework established in our previous study.[29] Specifically, ischemia-reperfusion injury-acute kidney injury (IRI-AKI) model was established by bilateral ligation of the renal arteries under anesthesia with 50 mg/kg sodium pentobarbital. Bilateral flank incisions were performed to isolate and clamp the renal arteries with noninvasive microvascular clips at 37 °C for 35 min. The control group experienced an identical surgical procedure without arterial ligation. Mice were euthanized 12, 24, or 48 h after reperfusion, and then heart blood samples were analyzed for SCr and blood urea nitrogen (BUN). Kidney tissue was procured after cardiac perfusion with precooled saline. All experiments were conducted in strict adherence to the guidelines for the care and use of laboratory animals established by the National Institutes of Health, and were approved by the Animal Ethics Committee of Henan Eye Hospital/Henan Eye Institute.

Histology and Renal Function

Kidney tissues were fixed in 4% formaldehyde, dehydrated, embedded in paraffin, sectioned, and stained with hematoxylin and eosin (H&E). SCr and BUN levels were quantified utilizing commercial kits from Jiancheng Bioengineering Institute (Nanjing, China) per the supplier's protocols.

Tubular Injury Score

After H&E staining of renal tissue, tubular injury was evaluated based on the loss of brush borders, tubular dilation, cast formation, and tubular necrosis, following established methods and grading criteria.[30] Ten high-power fields (magnification ×200) were randomly selected, with five fields from the renal cortex and five from the corticomedullary junction. Each field was scored on a scale from 0 to 5. All assessments were conducted by two nephropathology experts using a square grid technique for blinded scoring.

Western Blot (WB)

Kidney samples were lysed with RIPA buffer comprising cocktail inhibitors for 30 min on ice. Specimens were separated by spinning at 12,000 rpm for 15 min in a 4 °C environment. Protein levels were quantified utilizing a BCA protein measurement kit. WB analysis was executed employing 30 μg of protein per specimen according to standard protocols. Primary antibodies against EGR1 (Proteintech, 22008-1-AP, 1:1000), CEBPD (Invitrogen, PA5-75232, 1:1000), HSPA1A (Invitrogen, PA5-34772, 1:5000), HSPA1B (Invitrogen, PA5-28369, 1:1000), and RHOB (CST, 63876S, 1:1000) were used. For quantitation, protein levels were normalized.

Immunohistochemistry (IHC)

Paraffin-embedded kidney tissue blocks were cut into 5 μm sections. These sections underwent dewaxing with xylene and subsequent rehydration utilizing an ethanol concentration gradient. Antigen retrieval was executed by boiling sections in sodium citrate buffer for 15 min. Once cooled to ambient temperature, a 3% H_2O_2 solution was applied for 10 min to inhibit endogenous peroxidase activity. Sections were then blocked with 5% BSA for 30 min before overnight incubation at 4 °C with primary antibodies. Following phosphate buffer saline rinse, the sections underwent incubation with secondary antibodies at ambient temperature for 1 h. DAB staining was used for detection and quantitation. Hematoxylin was employed to stain nuclei.

Statistical Analysis

All data processing and graphical representations were conducted utilizing R version 4.3.1 and GraphPad Prism 9.0 software. WB images were processed using Image J software. To assess differences in continuous variables between two groups, the Wilcoxon test or *t*-test was applied as appropriate. In cases involving comparisons across multiple groups, one-way analysis of variance was employed. Pearson's correlation coefficient was used to evaluate the relationships between variables. $P < 0.05$ was considered statistically significant.

Results

Single-Cell Transcriptomic Atlases and Cell Typing

To identify the genes most indicative of PANoptosis, we analyzed scRNA-seq data. After removing batch effects using the Harmony algorithm, cells from different samples were evenly distributed (Figure 1A), indicating that the data were suitable for downstream analysis. Using FindClusters (resolution = 0.8), 25,684 cells were clustered into 29 groups (Figure 1B). Cellular annotation was executed utilizing classical marker genes and classified into 14 types (Figure 1C). Figure 1D illustrates the abundances of these types between AKI and normal kidney tissue. In AKI tissue, PT cells, loop of Henle (LOH) cells, natural killer T (NKT) cells, macrophages (MC), monocytes (MON), B cells and mesangial cells (MES) were more abundant than in normal tissue, whereas intercalated cells (IC), distal tubule (DT) cells, endothelial cells (EC), smooth muscle cells (SMC), fibroblasts (FIB), and podocytes (POD) were less abundant. Bubble (Figure 1E) and UMAP (Figure 1F) plots revealed distinct differences in marker gene expression among cell types, confirming the accuracy of the annotations.

Next, we performed GO enrichment analysis for each cell type (Figure 2). For example, DEGs in PC cells exhibited significant enrichment in pathways linked to hypoxia and renal development, whereas those in PT cells were strongly associated with responses to toxins and heavy metal ions. These observations contribute to our comprehension of diverse cellular categories and their functions.

Identifying PANoptosis-Related Genes from Single-cell Transcriptomes

To ascertain the role of PANoptosis in AKI, we initially evaluated gene expression variation at the overall level. Box plots illustrate scaled average expression levels of apoptosis, pyroptosis, and necroptosis in different cell samples. The transcription of genes linked to these forms of cell death was significantly upregulated in AKI than in normal tissues (Figure 3A–C). Subsequently, the AUCell, UCell, AddModuleScore, singscore, and ssgsea algorithms were employed to produce activity scores of apoptosis, pyroptosis, and necroptosis in each cell (Figure 3D–I). These analyses indicated heterogeneity in cell-death activities. Based on median scores (Figure 4A–C), cells were classified into high- and low-activity cohorts (Figure 4D–F). Notably, despite the different modes of cell death, high- and low-activity cells grouped according to apoptosis, pyroptosis, and necroptosis showed considerable similarities. Differential expression analysis was executed to screen for DEGs between groups (Figure 4G–I). Ultimately, by integrating and intersecting DEGs from the three modes of cell death (Supplementary Tables S3–S5), we identified 48 PANoptosis-related genes, among which 35 exhibited elevated expression and 13 showed diminished expression (Figure 4J–L and Supplementary Table S6).

Expression of PANoptosis-Related Genes in Bulk Data

GSVA examination of bulk data suggested that AKI kidney tissue exhibited higher levels of apoptosis, pyroptosis, and necroptosis than normal kidney tissue (Figure 5A–C). Although the differences in necroptosis were not statistically significant, a comparable upward pattern was noted, suggesting the involvement of PANoptosis in the progression of AKI. Furthermore, we identified the distinctions in the expression of these PANoptosis-related genes between the AKI and normal groups at the bulk level (Figure 5D–F and Supplementary Table S7). GO and DO functional enrichment analyses were conducted to investigate the potential functions of these genes. GO analysis demonstrated that these genes are linked to biological processes, encompassing apoptosis, ATP metabolism, neutrophil activation, and oxidative phosphorylation (Figure 5G). DO analysis indicated that these genes are primarily linked to diverse kidney diseases and urological cancers (Figure 5H).

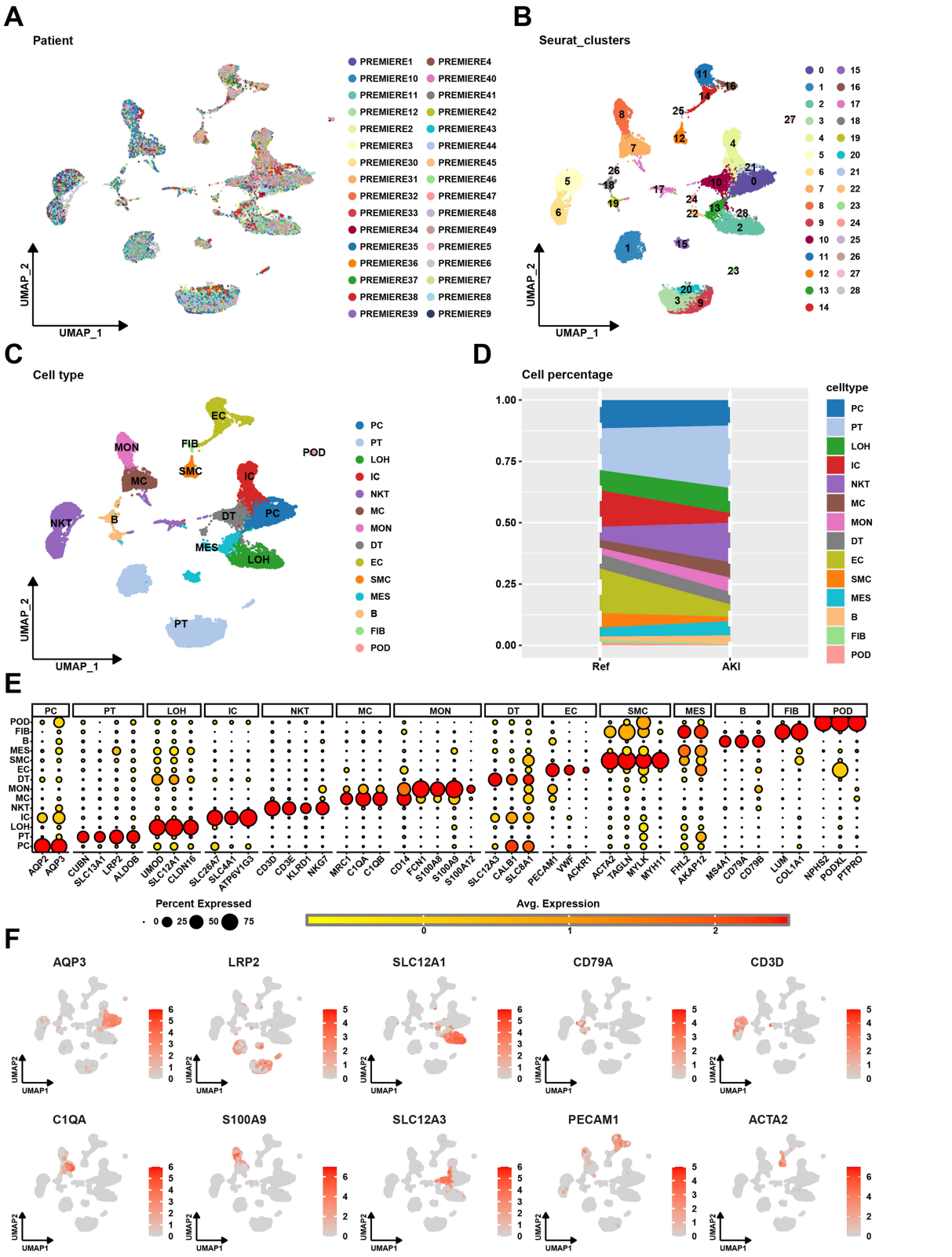

Figure 1 Single-cell transcriptome data preprocessing and cellular annotation. (**A**) The cell distribution of the samples showed no significant batch effect. (**B**) The results of UMAP plot indicated that all cells were finely classified into 29 clusters. (**C**) The UMAP plots of cells from all scRNA-seq samples, colored by cell-type annotation. (**D**) Cell proportion of different cell types in the tissues of normal and AKI patients. (**E**) Dot plot showing representative marker genes for each cell type. (**F**) Typical marker genes for each cell group.

 https://doi.org/10.2147/JIR.S525222

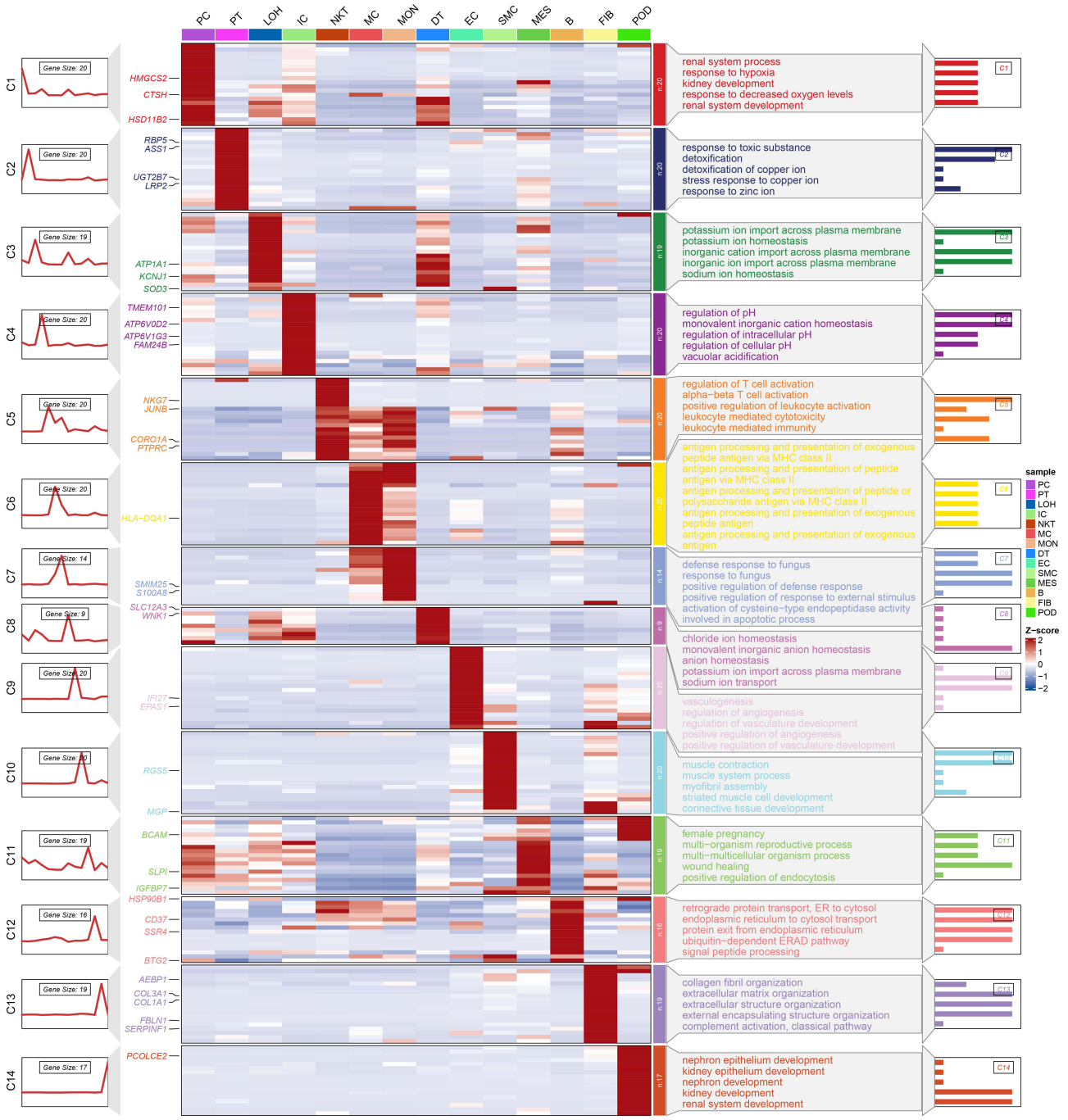

Figure 2 The relationship between the marker genes of each type of cells, along with the relevant pathways enriched by GO analysis.

Pinpointing Optimal Feature Genes

Seven machine-learning algorithms were employed. Using the RF algorithm, 19 key genes with importance scores of > 1 were selected from the PANoptosis-related gene list (Figure 6A and Supplementary Table S8). The GBM algorithm identified 22 key genes with importance scores > 0.1 (Figure 6B and Supplementary Table S9). The SVM-REF algorithm identified 16 key genes (Figure 6C and Supplementary Table S10), whereas the DT algorithm identified 7 key genes (Figure 6D and Supplementary Table S11). The XGBoost algorithm identified 26 key genes with importance scores > 0.1 (Figure 6E and Supplementary Table S12). The Boruta algorithm filtered irrelevant features, resulting in 25 key genes (Figure 6F and Supplementary Table S13). The LASSO algorithm identified 26 key genes (Figure 6G and Supplementary

https://doi.org/10.2147/JIR.S525222

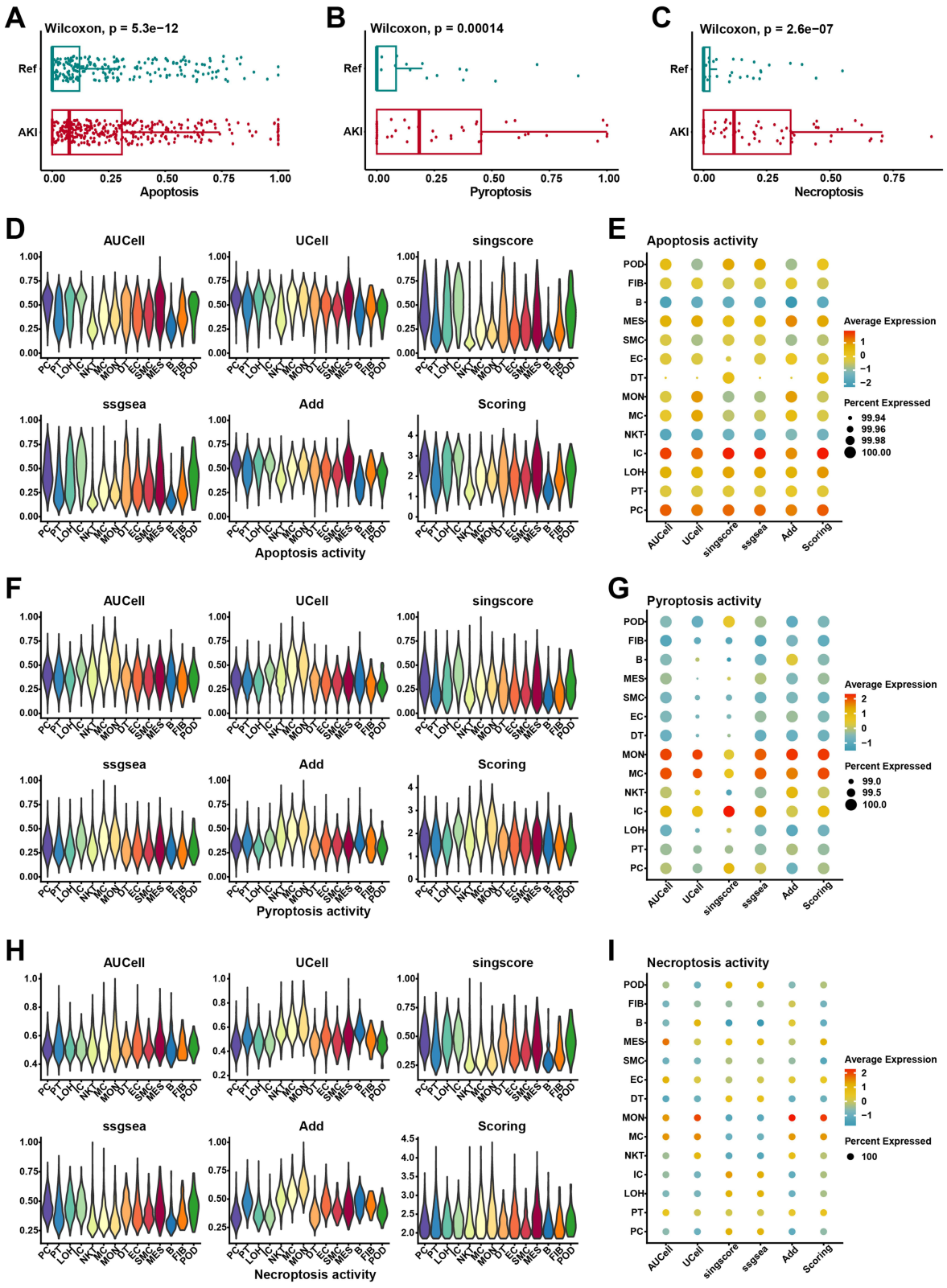

Figure 3 Single-cell analysis revealed the heterogeneity of PANoptosis in AKI. (**A**–**C**) Boxplots showing the scaled mean expression of apoptosis, pyroptosis and necroptosis signatures in cells from different sample groups. (**D**–**I**) Violin plot and Bubble plot showing enrichment scores of apoptosis (**D** and **E**), pyroptosis (**F** and **G**) and necroptosis (**H** and **I**) gene sets for each cell type using AUCell, UCell, singscore, ssgsea, AddModulescore, and Scoring score.

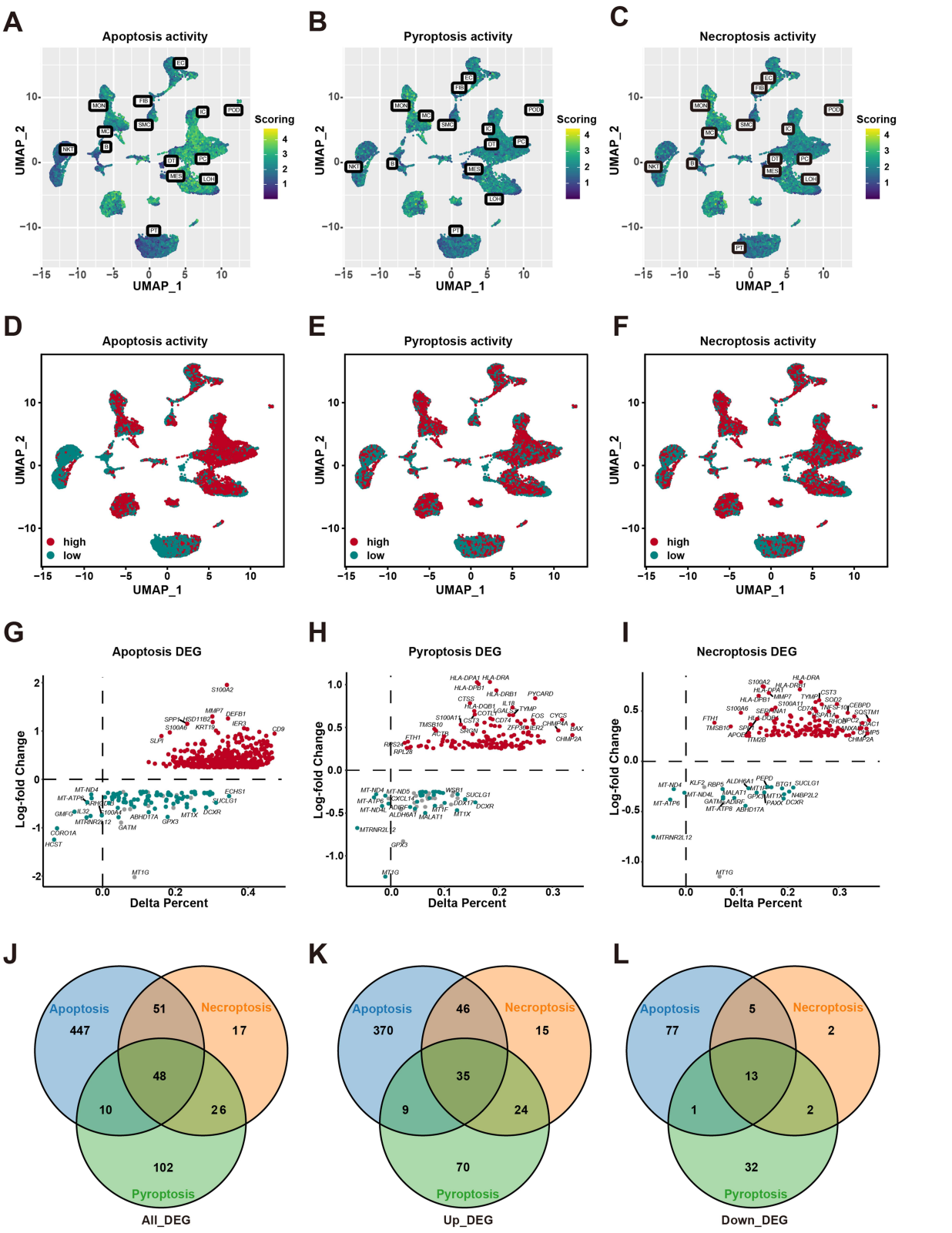

Figure 4 Identification of PANoptosis-related gene list in AKI. (**A**–**C**) The scoring score represented the activity of apoptosis, pyroptosis, and necroptosis in individual cells, visualized in a gradient color scheme. (**D**–**F**) Grouping of cells based on scoring score of apoptosis, pyroptosis and necroptosis. (**G**) Percentage difference (Delta means percent of cells) and log-fold change based on the Wilcoxon rank-sum test results for DEGs between high and low apoptosis cells. (**H**) Percentage difference and log-fold change based on the Wilcoxon rank-sum test results for DEGs between high and low pyroptosis cells. (**I**) Percentage difference and log-fold change based on the Wilcoxon rank-sum test results for DEGs between high and low necroptosis cells. (**J**–**L**) Venn diagram displayed the 48 shared PANoptosis gene signature obtained by the three types of cell death patterns, with 35 upregulated DEGs (**K**) and 13 down-regulated DEGs (**L**).

https://doi.org/10.2147/JIR.S525222

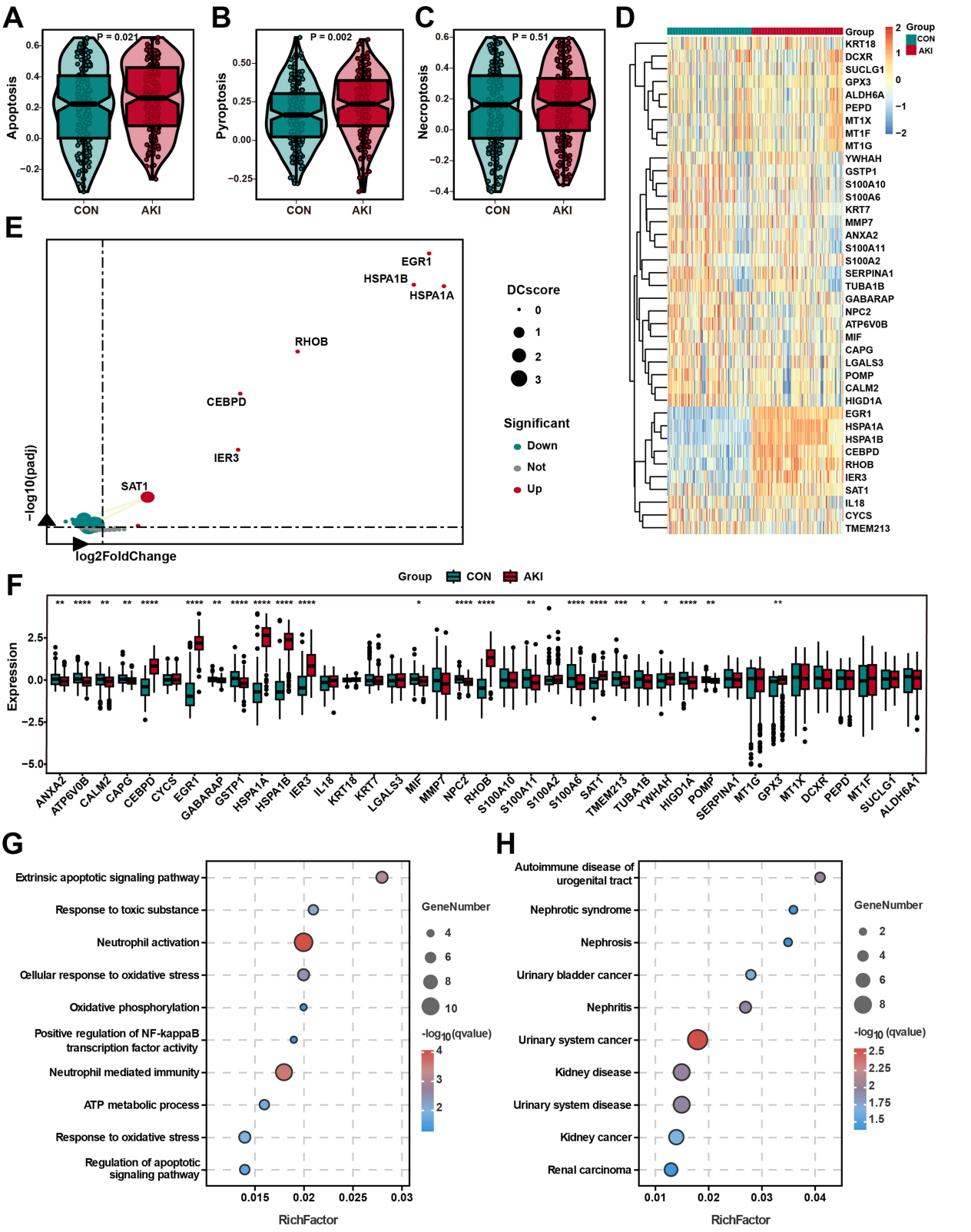

Figure 5 The expression of PANoptosis-related genes in bulk RNA-seq data of AKI. (**A**–**C**) The results of bulk RNA-seq dataset analysis showed that AKI tissues exhibited higher PANoptosis activity compared to normal kidney tissues. (**D**) Heat map of the PANoptosis-related genes. (**E**) Volcano plot of the PANoptosis-related genes. (**F**) Box plot demonstrated the results of the differential expression of PANoptosis-related genes at the bulk level between the normal and AKI groups. (**G**) Results of the GO analysis. (**H**) Results of the DO analysis. **P* < 0.05, ***P* < 0.01, ****P* < 0.001 and *****P* < 0.0001 compared with the control group.

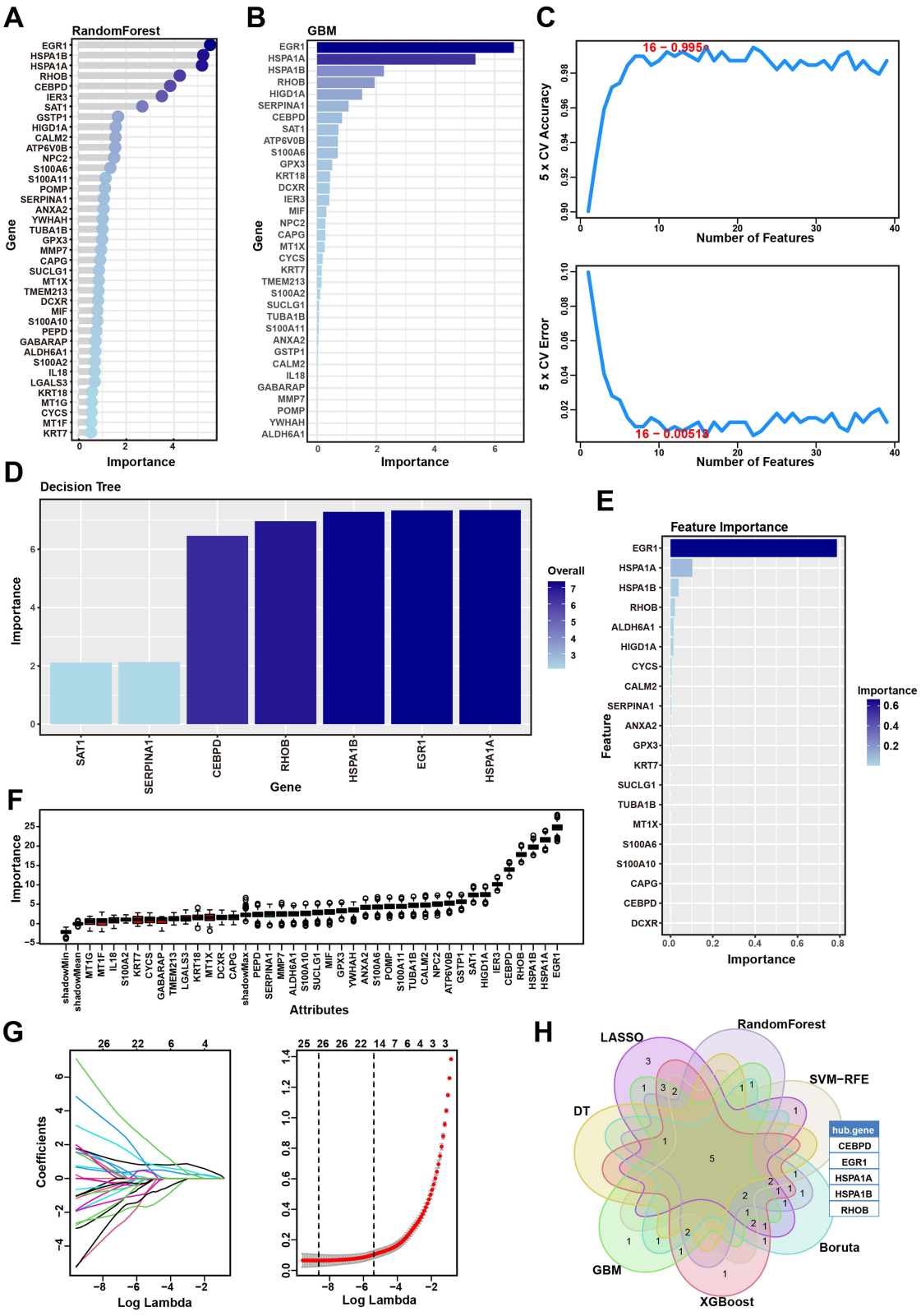

Figure 6 Machine learning algorithms evaluated the optimal feature genes. (**A**) The results of RF algorithm. (**B**) The results of GBM algorithm. (**C**) The results of SVM-REF algorithm. (**D**) The results of DT algorithm. (**E**) The results of XGboost algorithm. (**F**) The results of Boruta algorithm. (**G**) The results of LASSO algorithm. (**H**) Venn diagram to screen 5 overlapping genes presented in seven machine learning algorithms.

https://doi.org/10.2147/JIR.S525222

Table S14). By consolidating the genes identified by all seven algorithms, five optimal feature genes were determined: EGR1, CEBPD, HSPA1A, HSPA1B, and RHOB (Figure 6H).

Diagnostic Efficacy and Validation of Feature Genes

We noted substantial elevations in the expression of EGR1, CEBPD, HSPA1A, HSPA1B, and RHOB (Figure 7A–7E) in the AKI group relative to the control group (all $P < 0.001$). We then assessed the diagnostic value of these five feature genes. The areas under the curves (AUC) were 0.981 for EGR1, 0.920 for CEBPD, 0.968 for HSPA1A, 0.970 for HSPA1B, and 0.953 for RHOB (Figure 7F), demonstrating the accuracy of our analysis and strong diagnostic potential. Correlation analysis revealed that all the optimal genes exhibited significant positive associations with apoptosis, pyroptosis, and necroptosis (Figure 7G–7I). We verified the expression of the optimal feature genes in the scRNA-seq data. Specifically, CEBPD was predominantly expressed in IC, PC, MC, and SMC cells (Figure S2A–C). EGR1 was significantly expressed in IC, SMC, and FIB cells (Figure S2D–F). HSPA1A and HSPA1B were highly expressed in IC, PC, and MON cells (Figure S2G–L). RHOB was significantly expressed in IC, SMC, MC, and MES cells (Figure S2M–O). Additionally, the expression of optimal feature genes was validated in both high- and low-activity groups for all three types of cell death, with significantly higher expression observed in high-activity cells (Figure 7J–X).

GSEA of Optimal Feature Genes

To elucidate the potential biological relationships and functions between five optimized genes and PANoptosis in AKI, the GSEA was employed. After excluding normal samples, AKI samples were divided into two groups based on the median expression levels of these genes. The results demonstrated that apoptosis, pyroptosis, and necroptosis were notably enriched in the high-expression subgroups of all five optimal feature genes (Figure 8A–O), indicating a strong correlation between these genes and PANoptosis.

Construction of IRI-AKI Animal Model and Confirmation of Optimal Feature Genes

The workflow and grouping of animal models are shown in Figure 9A. We successfully established an IRI-AKI animal model and validated the expression of diagnostic genes utilizing WB and IHC techniques. H&E staining revealed tubular necrosis with the extent of injury progressively worsening over time (Figure 9B and Figure S3A). Compared to the control group, SCr, and BUN levels were elevated, demonstrating a significant time-effect relationship (Figure 9C). These findings confirm the successful establishment of the model. WB results indicated increased expression of EGR1, CEBPD, HSPA1A, HSPA1B, and RHOB post-AKI, consistent with our previous analyses (Figure 9D–E). IHC showed nuclear localization of CEBPD and EGR1 and cytoplasmic localization of HSPA1A, HSPA1B, and RHOB, with all genes showing heightened expression in AKI, particularly in damaged cells (Figure 9F). To further validate the relationship between feature genes and PANoptosis, we evaluated the correlation between the expression of five feature genes and tubular injury scores. The results indicated a significant positive correlation between the expression of all five genes and tubular injury scores (Figure S3B–F).

Discussion

The high incidence and severe consequences of AKI pose a significant global public health challenge.[31] Common causes of AKI encompass ischemia-reperfusion, sepsis, nephrotoxic drugs, and urinary-tract obstruction. Although these causes differ mechanistically, they share the common features of uncontrolled inflammation and PCD.[32]

PANoptosis represents a highly synchronized and dynamic form of inflammatory cell death that integrates key molecular aspects of pyroptosis, apoptosis, and necroptosis.[33] PANoptosis is primarily modulated by a multifaceted macromolecular complex known as the PANoptosome, whose composition varies depending on cellular triggering factors. This complex, which incorporates the main regulatory factors of the three cell death pathways, can initiate cell death and PAMPs, DAMPs, or other danger signals.[34] PANoptosis is implicated in multiple diseases, encompassing metabolic, neurological, infectious, cancerous, inflammatory, and immune disorders. Manipulation of key molecules within this pathway is likely to provide new therapeutic opportunities.[35] As the precise role of PANoptosis in AKI remains unclear, our goal was to integrate scRNA-seq and bulk RNA-seq data to more comprehensively analyze the characteristics of PANoptosis in AKI and identify new therapeutic targets.

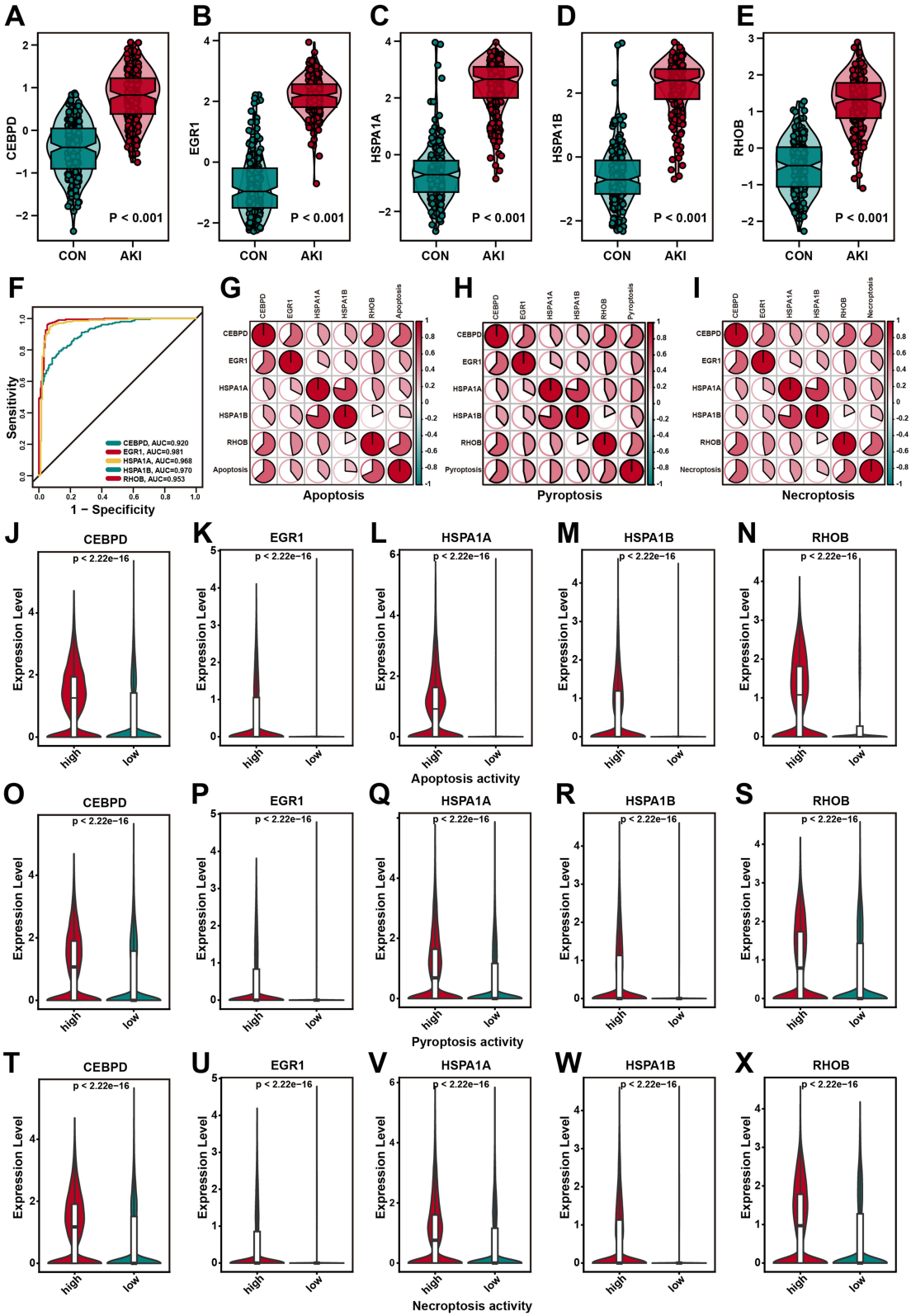

Figure 7 The expression of the optimal feature genes. (**A**–**E**) The expression of 5 hub genes were significantly elevated in the AKI group. (**F**) ROC curves estimating the diagnostic performance of the hub genes. (**G**–**I**) The correlation of hub genes with apoptosis, pyroptosis, and necroptosis. (**J**–**N**) Expression of hub genes in high and low apoptosis subgroups. (**O**–**S**) Expression of hub genes in high and low pyroptosis subgroups. (**T**–**X**) Expression of hub genes in high and low necroptosis subgroups.

https://doi.org/10.2147/JIR.S525222

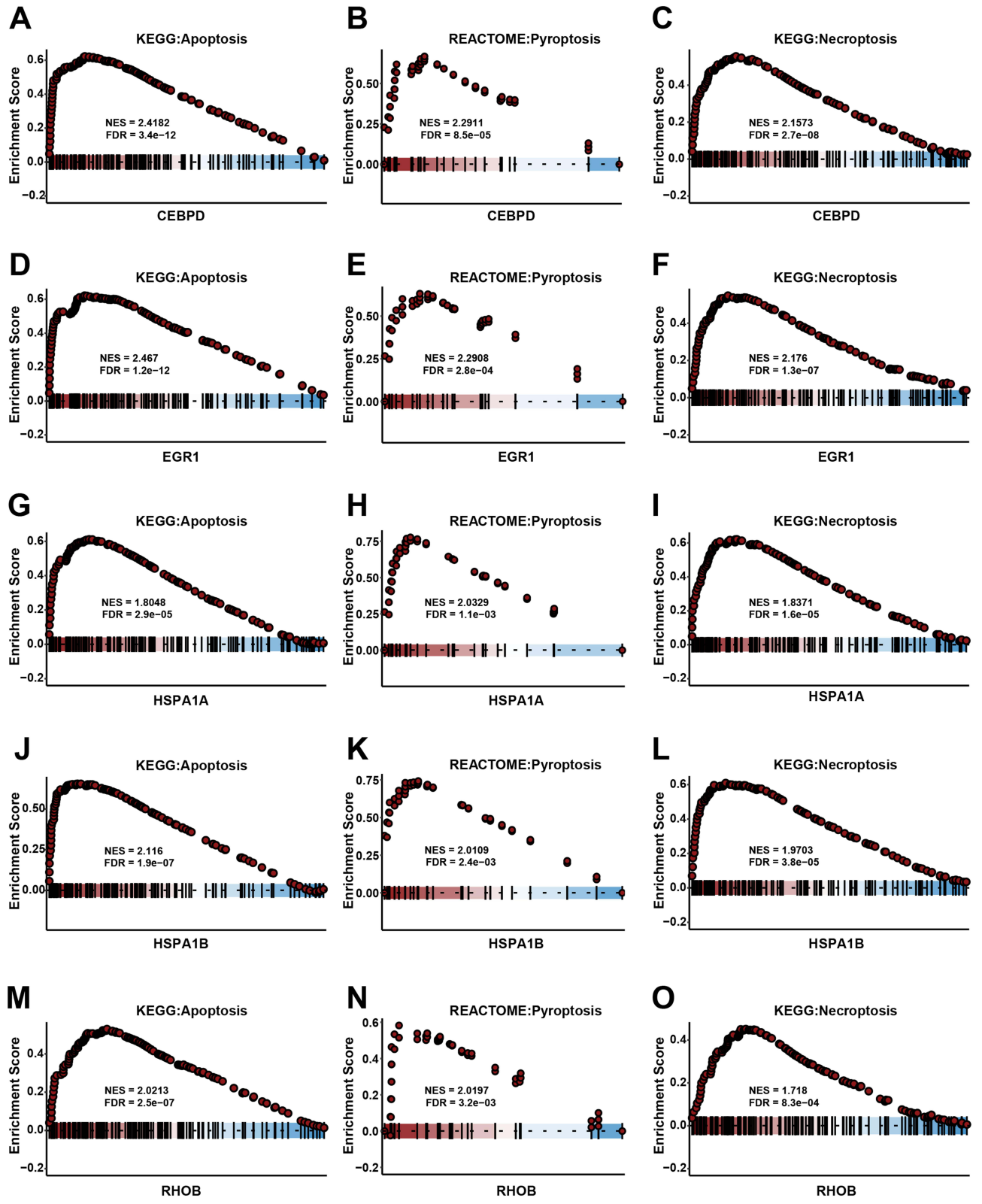

Figure 8 GSEA results for optimal feature genes showed significant enrichment of PANoptosis pathway. (**A–C**) The results of single-gene GSEA for CEBPD. (**D–F**) The results of single-gene GSEA for EGR1. (**G–I**) The results of single-gene GSEA for HSPA1A. (**J–L**) The results of single-gene GSEA for HSPA1B. (**M–O**) The results of single-gene GSEA for RHOB.

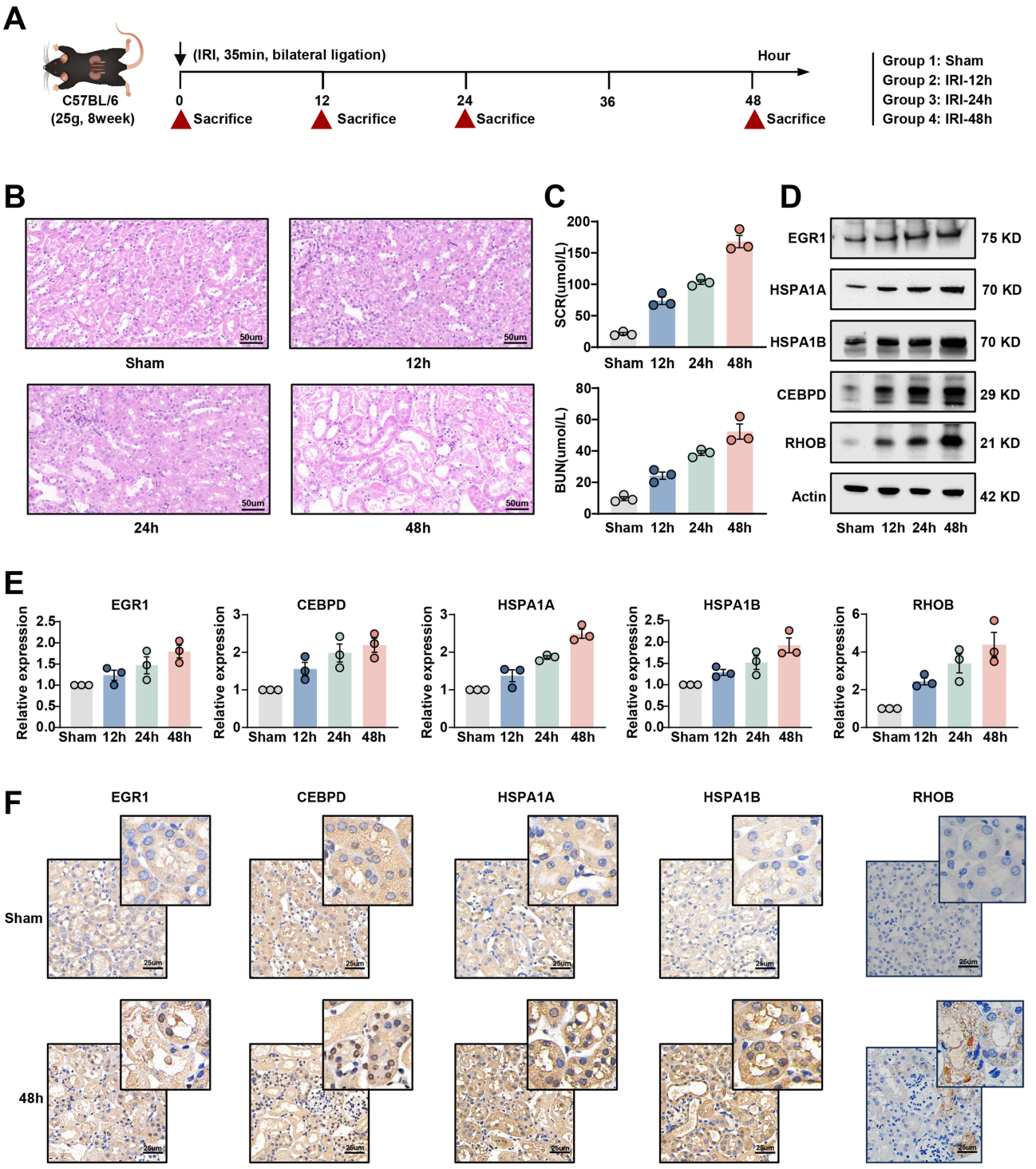

Figure 9 The results of experimental verification of IRI-AKI mouse model. (**A**) Diagram and grouping of animal experiments. (**B**) HE staining of the mouse kidney sections in the IRI-AKI mouse models at the reperfusion time of 12 h, 24 h, or 48 h (Scale bar: 50 μm). (**C**) The concentrations of SCr and BUN in the mouse models at the reperfusion time of 12 h, 24 h or 48 h. (**D**) The expression levels of optimal feature genes detected with WB assays in IRI-AKI mouse model. (**E**) The quantitative results of the relative expression levels of optimal feature genes. (**F**) IHC staining of optimal feature genes between the sham and AKI mouse kidneys (Scale bar: 25 μm).

With the swift growth in high-throughput sequencing data and the advancement of artificial intelligence, leveraging big data to explore disease diagnostic markers and therapeutic targets has become a crucial research focus.[36] Previous transcriptomic studies on AKI have primarily utilized bulk RNA-seq data and often overlooked cellular heterogeneity. The scRNA-seq studies on AKI have mainly focused on identifying and characterizing cellular components, discovering

https://doi.org/10.2147/JIR.S525222

new cell subtypes, and investigating intercellular heterogeneity, with limited assessments of disease-specific pathways. Moreover, small sample sizes with scRNA-seq have impeded the assessment of the prognostic and diagnostic effectiveness of specific genes.

Our analysis revealed that PANoptosis levels were notably elevated in AKI kidney tissues relative to normal tissues. GSVA pathway scoring of the bulk transcriptomic data further indicated that PANoptosis was activated in AKI patients. We assessed the heterogeneity of PANoptosis between AKI and normal kidney tissues using scRNA-seq profiles. It was noteworthy to note that activity scores for apoptosis, pyroptosis, and necroptosis exhibited significant heterogeneity across different cell types. Apoptotic activity scores were predominantly elevated in IC, while pyroptotic and necroptotic activity scores were mainly enriched in MON and MC. This finding contrasts with previous research that primarily focused on the role of PT cell death in AKI.[37] Recent research suggests that the death of IC may be pivotal in the onset and progression of AKI. Following surgery, distant organ injury, sepsis, or localized renal damage, IC emerge as critical mediators of renal inflammation and AKI.[38] In IRI-AKI, MMP9 protects IC from apoptosis by releasing stem cell factor.[39] Regarding the involvement of MON and MC in AKI, studies indicate that these cells undergo pyroptosis in an "altruistic" manner, recruiting inflammatory cells and promoting AKI progression. However, the underlying molecular mechanisms require further exploration.[40] Given that PANoptosis encompasses features of pyroptosis, apoptosis, and necroptosis, we identified a candidate gene set associated with AKI-related PANoptosis by intersecting genes that differentiate between these three cell death modes at the single-cell level. Functional enrichment analysis of the candidate gene set further validated this analytical approach.

To identify optimal feature genes, machine-learning methods were employed for feature selection and core gene acquisition. As a branch of artificial intelligence, machine learning detects patterns and correlations within data, enabling the accurate prediction of future events.[41] Traditionally, the identification of diagnostic biomarkers for AKI has relied on singular machine-learning algorithms or frameworks, which often constrain the resilience and accuracy of predictions. In this study, a combination of machine-learning algorithms was used to filter the candidate gene set, leading to the identification of five core genes associated with PANoptosis in AKI: EGR1, CEBPD, HSPA1A, HSPA1B, and RHOB. Validation using bulk transcriptomic data revealed elevated expression of these genes in the AKI group. ROC curve analysis showed that all five genes had an AUC value greater than 0.9, indicating their potential as diagnostic biomarkers for AKI. Additionally, GSEA and in vivo experiments were performed. GSEA results demonstrated significant associations between all five genes and PANoptosis. Using an IRI-AKI animal model, the tissue localization and expression of the five core genes were further validated through WB and IHC. Moreover, the correlation analysis between the relative expression of characteristic genes and tubular injury scores further reinforced the association between these genes and PANoptosis.

EGR1, early growth response protein 1, is a transcription factor expressed in response to a wide range of non-lethal external stimuli.[42] Upon activation, it forms complexes with response factors in serum and binds to GC-rich regions of DNA through three zinc-finger domains, regulating the transcription of numerous downstream genes. EGR1 assumes a vital function in cellular processes encompassing proliferation, differentiation, apoptosis, and inflammation.[43] Contemporary investigations have demonstrated that during AKI, autophagy can stimulate EGR1 through the MAPK/ERK pathway, leading to FGF2 secretion, fibroblast activation, and fibrosis.[44] Additionally, transient upregulation of EGR1 signaling enhances renal repair during AKI by triggering SOX9+ renal tubular cells.[45] These observations indicate that EGR1 has a considerable impact on AKI.

HSPA1A and HSPA1B, key members of the Hsp70 family, are essential cellular stress-protective proteins. They have been shown to be involved in regulating apoptosis and proliferation, as well as in the activation of transcription factors and protein degradation.[46,47] Nevertheless, Hsp70's function in AKI is yet to be elucidated. RHOB, a small GTPase belonging to the Ras superfamily, undergoes farnesylation or geranylgeranylation, with its isoprenylation status influencing its function.[48] Farnesylated RhoB typically localizes to the cell membrane, promoting cell growth, mediating Ras effects on the actin cytoskeleton, and activating NF-κB. Conversely, geranylgeranylated RhoB concentrates in endosomes and triggers apoptosis. Collectively, these characteristics contribute to RhoB's involvement in modulating cell proliferation, death, and inflammation.[49] CEBPD, a constituent of the C/EBP transcription factor family, is normally present at low levels under physiological conditions, but its expression increases rapidly in response to external stimuli, such as

immune activation and inflammation. Recent investigations have demonstrated that CEBPD exerts regulatory effects on cell death and inflammation. It promotes LPS-induced inflammatory responses by inducing TLR4 expression, inhibiting FBXW7 expression,[50] and facilitating M1-like polarization of macrophages during inflammation.[51] In PCD, CEBPD expression in cervical cancer induces apoptosis through transcriptional regulation of the pro-apoptotic genes PPARG2 and GADD153.[52] However, the specific mechanisms linking the identified optimal feature genes to PANoptosis remain unclear. The above literature review systematically analyzed the molecular functions of the identified feature genes, suggesting their potential role in regulating PANoptosis in AKI; however, further experimental validation is required.

Admittedly, there are limitations to our study. First, because renal biopsy is not a standard practice in the clinical management of AKI, we were unable to obtain human tissue samples for validation. Therefore, our research was restricted to validation using a single animal model of AKI. Additionally, in vitro experiments to validate the functional roles of core genes in AKI are lacking. Second, the potential of the identified genes as diagnostic biomarkers must be confirmed through prospective clinical trials.

Conclusions

In summary, this study defined a PANoptosis-related gene set based on AKI scRNA-seq profiles. By combining this gene set with bulk RNA-seq data, multiple machine-learning algorithms were employed to ascertain optimal feature genes. Our results not only introduce new diagnostic markers for AKI, but also highlight potential therapeutic targets, which may significantly enhance the management and treatment of AKI.

Abbreviations

AKI, acute kidney injury; SCr, serum creatinine; PT, proximal tubular; PCD, programmed cell death; RNA-seq, RNA sequencing; scRNA-seq, single-cell RNA sequencing; DEGs, differentially expressed genes; GEO, Gene Expression Omnibus; GSVA, gene set variation analysis; GO, gene ontology; DO, disease ontology; XGBoost, eXtreme Gradient Boosting; RF, Random Forest; LASSO, Least Absolute Shrinkage and Selection Operator; SVM-RFE, Support Vector Machine Recursive Feature Elimination; DT, Decision Tree; GBM, Gradient Boosting Machine; ROC, receiver operating characteristic; GSEA, Gene Set Enrichment Analysis; IRI-AKI, ischemia-reperfusion injury- acute kidney injury; BUN, blood urea nitrogen; H&E, hematoxylin and eosin; WB, Western blot; IHC, immunohistochemistry; LOH, loop of Henle; NKT, natural killer T; MC, macrophages; MON, monocytes; MES, mesangial cells; PC, principal cells; IC, intercalated cells; DT, distal tubule; EC, endothelial cells; SMC, smooth muscle cells; FIB, fibroblasts; POD, podocytes. AUC, area under the curve.

Data Sharing Statement

The datasets analyzed during the current study are available in the GEO database (https://www.ncbi.nlm.nih.gov/geo/). The original contributions presented in the study are included in the article/Supplementary Materials. All data are available from the corresponding author on reasonable request.

Ethics Approval and Consent to Participate

All experiments were performed in strict compliance with the National Institutes of Health guidelines for the care and use of laboratory animals and were approved by the Animal Ethics Committee of Henan Eye Hospital/Henan Eye Institute (approval number HNEECA–2020–12). Ethical approval was not required for the use of human sequencing data derived from public databases in accordance with the local legislation and institutional requirements.

Acknowledgments

We are grateful to the contributors to the public databases used in this study and the reviewers for their constructive and helpful comments.

Author Contributions

All authors made a significant contribution to the work reported, whether that is in the conception, study design, execution, acquisition of data, analysis and interpretation, or in all these areas; took part in drafting, revising or critically reviewing the article; gave final approval of the version to be published; have agreed on the journal to which the article has been submitted; and agree to be accountable for all aspects of the work.

Funding

This work was supported by the National Natural Science Foundation of China (No.82100731), the Medical Science and Technology Research Youth Project of Henan Provincial Health Commission (SBGJ202103004), the Joint Fund Project of Henan Provincial Science and Technology Research and Development Plan (No. 225200810101), the Henan Province Science and Technology Attack Plan Project (LHGJ20210058), Natural Science Foundation of Henan Province (No. 202300410401) and Funding of Zhongyuan Scholars of Henan Provincial Health Commission (No. 224000510005).

Disclosure

The authors declare that they have no conflicts of interest in this work.

References

1. Moledina DG, Hall IE, Thiessen-Philbrook H, et al. Performance of Serum Creatinine and Kidney Injury Biomarkers for Diagnosing Histologic Acute Tubular Injury. *Am J Kidney Dis*. 2017;70(6):807–816. doi:10.1053/j.ajkd.2017.06.031
2. Sohaney R, Yin H, Shahinian V, et al. In-Hospital and 1-Year Mortality Trends in a National Cohort of US Veterans with Acute Kidney Injury. *Clin J Am Soc Nephrol*. 2022;17(2):184–193. doi:10.2215/cjn.01730221
3. Wang Q, Tang Y, Zhou J, et al. A prospective study of acute kidney injury in the intensive care unit: development and validation of a risk prediction model. *J Transl Med*. 2019;17(1):359. doi:10.1186/s12967-019-2118-6
4. Dahlerus C, Segal JH, He K, et al. Acute Kidney Injury Requiring Dialysis and Incident Dialysis Patient Outcomes in US Outpatient Dialysis Facilities. *Clin J Am Soc Nephrol*. 2021;16(6):853–861. doi:10.2215/cjn.18311120
5. Brar S, Ye F, James MT, et al. Association of Angiotensin-Converting Enzyme Inhibitor or Angiotensin Receptor Blocker Use With Outcomes After Acute Kidney Injury. *JAMA Intern Med*. 2018;178(12):1681–1690. doi:10.1001/jamainternmed.2018.4749
6. Moerke C, Jaco I, Dewitz C, et al. The anticonvulsive Phenhydan® suppresses extrinsic cell death. *Cell Death Differ*. 2019;26(9):1631–1645. doi:10.1038/s41418-018-0232-2
7. Bhargava P, Schnellmann RG. Mitochondrial energetics in the kidney. *Nat Rev Nephrol*. 2017;13(10):629–646. doi:10.1038/nrneph.2017.107
8. Tábara LC, Poveda J, Martin-Cleary C, et al. Mitochondria-targeted therapies for acute kidney injury. *Expert Rev Mol Med*. 2014;16:e13. doi:10.1017/erm.2014.14
9. Bedoui S, Herold MJ, Strasser A. Emerging connectivity of programmed cell death pathways and its physiological implications. *Nat Rev Mol Cell Biol*. 2020;21(11):678–695. doi:10.1038/s41580-020-0270-8
10. Privitera G, Rana N, Armuzzi A, et al. The gasdermin protein family: emerging roles in gastrointestinal health and disease. *Nat Rev Gastroenterol Hepatol*. 2023;20(6):366–387. doi:10.1038/s41575-023-00743-w
11. Pefanis A, Ierino FL, Murphy JM, et al. Regulated necrosis in kidney ischemia-reperfusion injury. *Kidney Int*. 2019;96(2):291–301. doi:10.1016/j.kint.2019.02.009
12. Christgen S, Tweedell RE, Kanneganti TD. Programming inflammatory cell death for therapy. *Pharmacol Ther*. 2022;232:108010. doi:10.1016/j.pharmthera.2021.108010
13. Kesavardhana S, Kuriakose T, Guy CS, et al. ZBP1/DAI ubiquitination and sensing of influenza vRNPs activate programmed cell death. *J Exp Med*. 2017;214(8):2217–2229. doi:10.1084/jem.20170550
14. Malireddi RKS, Kesavardhana S, Kanneganti TD. ZBP1 and TAK1: master Regulators of NLRP3 Inflammasome/Pyroptosis, Apoptosis, and Necroptosis (PAN-optosis). *Front Cell Infect Microbiol*. 2019;9:406. doi:10.3389/fcimb.2019.00406
15. Wei S, Wu L, Xiang Z, et al. EIF2AK2 protein targeted activation of AIM2-mediated PANoptosis promotes sepsis-induced acute kidney injury. *Ren Fail*. 2024;46(2):2403649. doi:10.1080/0886022x.2024.2403649
16. Xu C, Wang Q, Du C, et al. Histone deacetylase-mediated silencing of PSTPIP2 expression contributes to aristolochic acid nephropathy-induced PANoptosis. *Br J Pharmacol*. 2024;181(9):1452–1473. doi:10.1111/bph.16299
17. Jiang L, Chen H, Pinello L, et al. GiniClust: detecting rare cell types from single-cell gene expression data with Gini index. *Genome Biol*. 2016;17(1):144. doi:10.1186/s13059-016-1010-4
18. Klocke J, Kim SJ, Skopnik CM, et al. Urinary single-cell sequencing captures kidney injury and repair processes in human acute kidney injury. *Kidney Int*. 2022;102(6):1359–1370. doi:10.1016/j.kint.2022.07.032
19. Chen G, Qi H, Jiang L, et al. Integrating single-cell RNA-Seq and machine learning to dissect tryptophan metabolism in ulcerative colitis. *J Transl Med*. 2024;22(1):1121. doi:10.1186/s12967-024-05934-w
20. Lake BB, Menon R, Winfree S, et al. An atlas of healthy and injured cell states and niches in the human kidney. *Nature*. 2023;619(7970):585–594. doi:10.1038/s41586-023-05769-3
21. Damman J, Bloks VW, Daha MR, et al. Hypoxia and Complement-and-Coagulation Pathways in the Deceased Organ Donor as the Major Target for Intervention to Improve Renal Allograft Outcome. *Transplantation*. 2015;99(6):1293–1300. doi:10.1097/tp.0000000000000500

22. Xu Y, Hua J, Que H, et al. Identification of PANoptosis-related signature reveals immune infiltration characteristics and immunotherapy responses for renal cell carcinoma. *BMC Cancer*. 2024;24(1):292. doi:10.1186/s12885-024-12067-2
23. Hänzelmann S, Castelo R, Guinney J. GSVA: gene set variation analysis for microarray and RNA-seq data. *BMC Bioinf*. 2013;14(1):7. doi:10.1186/1471-2105-14-7
24. Butler A, Hoffman P, Smibert P, et al. Integrating single-cell transcriptomic data across different conditions, technologies, and species. *Nat Biotechnol*. 2018;36(5):411–420. doi:10.1038/nbt.4096
25. Ritchie ME, Phipson B, Wu D, et al. limma powers differential expression analyses for RNA-sequencing and microarray studies. *Nucleic Acids Res*. 2015;43(7):e47. doi:10.1093/nar/gkv007
26. Zhao S, Wang Q, Ni K, et al. Combining single-cell sequencing and spatial transcriptome sequencing to identify exosome-related features of glioblastoma and constructing a prognostic model to identify BARD1 as a potential therapeutic target for GBM patients. *Front Immunol*. 2023;14:1263329. doi:10.3389/fimmu.2023.1263329
27. Andreatta M, Carmona SJ. UCell: robust and scalable single-cell gene signature scoring. *Comput Struct Biotechnol J*. 2021;19:3796–3798. doi:10.1016/j.csbj.2021.06.043
28. Wu T, Hu E, Xu S, et al. clusterProfiler 4.0: a universal enrichment tool for interpreting omics data. *Innovation*. 2021;2(3):100141. doi:10.1016/j.xinn.2021.100141
29. Liu W, Gan Y, Ding Y, et al. Autophagy promotes GSDME-mediated pyroptosis via intrinsic and extrinsic apoptotic pathways in cobalt chloride-induced hypoxia reoxygenation-acute kidney injury. *Ecotoxicol Environ Saf*. 2022;242:113881. doi:10.1016/j.ecoenv.2022.113881
30. Yang B, Lan S, Dieudé M, et al. Caspase-3 Is a Pivotal Regulator of Microvascular Rarefaction and Renal Fibrosis after Ischemia-Reperfusion Injury. *J Am Soc Nephrol*. 2018;29(7):1900–1916. doi:10.1681/asn.2017050581
31. Yang Q, Ren GL, Wei B, et al. Conditional knockout of TGF-βRII /Smad2 signals protects against acute renal injury by alleviating cell necroptosis, apoptosis and inflammation. *Theranostics*. 2019;9(26):8277–8293. doi:10.7150/thno.35686
32. Wilflingseder J, Willi M, Lee HK, et al. Enhancer and super-enhancer dynamics in repair after ischemic acute kidney injury. *Nat Commun*. 2020;11(1):3383. doi:10.1038/s41467-020-17205-5
33. Xiang Q, Geng ZX, Yi X, et al. PANoptosis: a novel target for cardiovascular diseases. *Trends Pharmacol Sci*. 2024;45(8):739–756. doi:10.1016/j.tips.2024.06.002
34. Pandeya A, Kanneganti TD. Therapeutic potential of PANoptosis: innate sensors, inflammasomes, and RIPKs in PANoptosomes. *Trends Mol Med*. 2024;30(1):74–88. doi:10.1016/j.molmed.2023.10.001
35. Lin JF, Hu PS, Wang YY, et al. Phosphorylated NFS1 weakens oxaliplatin-based chemosensitivity of colorectal cancer by preventing PANoptosis. *Signal Transduct Target Ther*. 2022;7(1):54. doi:10.1038/s41392-022-00889-0
36. Satam H, Joshi K, Mangrolia U, et al. Next-Generation Sequencing Technology: current Trends and Advancements. *Biolog*. 2023;12(7):997. doi:10.3390/biology12070997
37. Linkermann A, Chen G, Dong G, et al. Regulated cell death in AKI. *J Am Soc Nephrol*. 2014;25(12):2689–2701. doi:10.1681/asn.2014030262
38. Breton S, Brown D. Novel Proinflammatory Function of Renal Intercalated Cells. *Ann Nutr Metab*. 2018;72 Suppl 2(Suppl. 2):11–16. doi:10.1159/000488303
39. Bengatta S, Arnould C, Letavernier E, et al. MMP9 and SCF protect from apoptosis in acute kidney injury. *J Am Soc Nephrol*. 2009;20(4):787–797. doi:10.1681/asn.2008050515
40. de Roquetaillade C, Durand M, Beaucoté V, et al. Progression of Kidney Fibrosis after Sepsis: underestimated Role of Resident Macrophages and Recruited Monocytes. *J Am Soc Nephrol*. 2025. doi:10.1681/asn.0000000712
41. Hyer JM, Ejaz A, Tsilimigras DI, et al. Novel Machine Learning Approach to Identify Preoperative Risk Factors Associated With Super-Utilization of Medicare Expenditure Following Surgery. *JAMA Surg*. 2019;154(11):1014–1021. doi:10.1001/jamasurg.2019.2979
42. Wang W, Xiong Y, Ding X, et al. Cathepsin L activated by mutant p53 and Egr-1 promotes ionizing radiation-induced EMT in human NSCLC. *J Exp Clin Cancer Res*. 2019;38(1):61. doi:10.1186/s13046-019-1054-x
43. Chen F, Wang Y, Zhang W, et al. A Functional Polymorphism-Mediated Disruption of EGR1/ADAM10 Pathway Confers the Risk of Sepsis Progression. *mBio*. 2019;10(4):e01663–19. doi:10.1128/mBio.01663-19
44. Livingston MJ, Zhang M, Kwon SH, et al. Autophagy activates EGR1 via MAPK/ERK to induce FGF2 in renal tubular cells for fibroblast activation and fibrosis during maladaptive kidney repair. *Autophagy*. 2024;20(5):1032–1053. doi:10.1080/15548627.2023.2281156
45. Chen JW, Huang MJ, Chen XN, et al. Transient upregulation of EGR1 signaling enhances kidney repair by activating $SOX9^{+}$ renal tubular cells. *Theranostics*. 2022;12(12):5434–5450. doi:10.7150/thno.73426
46. Di G, Luo X, You W, et al. Proteomic analysis of muscle between hybrid abalone and parental lines Haliotis gigantea Reeve and Haliotis discus hannai Ino. *Heredity*. 2015;114(6):564–574. doi:10.1038/hdy.2014.124
47. Jain CV, Jessmon P, Barrak CT, et al. Trophoblast survival signaling during human placentation requires HSP70 activation of MMP2-mediated HBEGF shedding. *Cell Death Differ*. 2017;24(10):1772–1783. doi:10.1038/cdd.2017.104
48. Marlow LA, Reynolds LA, Cleland AS, et al. Reactivation of suppressed RhoB is a critical step for the inhibition of anaplastic thyroid cancer growth. *Cancer Res*. 2009;69(4):1536–1544. doi:10.1158/0008-5472.Can-08-3718
49. Komarova YA, Kruse K, Mehta D, et al. Protein Interactions at Endothelial Junctions and Signaling Mechanisms Regulating Endothelial Permeability. *Circ Res*. 2017;120(1):179–206. doi:10.1161/circresaha.116.306534
50. Balamurugan K, Sharan S, Klarmann KD, et al. FBXW7α attenuates inflammatory signalling by downregulating C/EBPδ and its target gene Tlr4. *Nat Commun*. 2013;4(1):1662. doi:10.1038/ncomms2677
51. Lai HY, Hsu LW, Tsai HH, et al. CCAAT/enhancer-binding protein delta promotes intracellular lipid accumulation in M1 macrophages of vascular lesions. *Cardiovasc Res*. 2017;113(11):1376–1388. doi:10.1093/cvr/cvx134
52. Pan YC, Li CF, Ko CY, et al. CEBPD reverses RB/E2F1-mediated gene repression and participates in HMDB-induced apoptosis of cancer cells. *Clin Cancer Res*. 2010;16(23):5770–5780. doi:10.1158/1078-0432.Ccr-10-1025